



An efficient and combined placental T_1 -ADC acquisition in pregnancies with and without pre-eclampsia

Jana Hutter^{1,2}   | Alison Ho³ | Laurence H. Jackson^{1,2} | Paddy J. Slator⁴ | Lucy C. Chappell³ | Joseph V. Hajnal^{1,2} | Mary A. Rutherford^{1,2}

¹Center for Medical Engineering, King's College London, London, UK

²Center for the Developing Brain, School of Biomedical Engineering and Imaging, King's College London, London, UK

³Academic Women's Health Department, King's College London, London, UK

⁴Centre for Medical Image Computing, Department of Computer Science, University College London, London, UK

Correspondence

Jana Hutter, Center for Medical Engineering, King's College London, London, UK.
Email: jana.hutter@kcl.ac.uk

Funding information

UKRI, Grant/Award Number: MR/T018119/1; National Institute of Child Health and Human Development, Grant/Award Number: 1U01HD087202-01; Wellcome Trust, Grant/Award Number: 201374/Z/16/Z

Purpose: To provide a new approach to jointly assess microstructural and molecular properties of the human placenta in vivo fast and efficiently and to present initial evidence in cohorts of healthy pregnancies and those affected by pre-eclampsia.

Methods: Slice and diffusion preparation shuffling, built on the previously proposed ZEBRA method, is presented as a robust and fast way to obtain T_1 and apparent diffusivity coefficient (ADC) values. Joint modeling and evaluation is performed on a cohort of healthy and pre-eclamptic participants at 3T.

Results: The datasets show the ability to obtain robust and fast T_1 -ADC measurements. Significant decay over gestation in T_1 (-11 ms/week, $P < .05$) and a trend toward significance in ADC (-0.23 mm²/week, $P = .08$) values can be observed in a control cohort. Values for the pre-eclamptic pregnancies show a negative trend for both ADC and T_1 .

Conclusions: The presented sequence allows the simultaneous acquisition of 2 of the most promising quantitative parameters to study placental insufficiency—identified individually as relevant in previous studies—in under 2 minutes. This allows dynamic assessment of physiological processes, reduced inconsistency in spatial comparisons due to reduced motion artefacts and opens novel avenues for analysis. Initial results in pre-eclamptic placentas, with depicted changes in both ADC and T_1 , illustrate its potential to identify cases of placental insufficiency. Future work will focus on expanding the field-of-view using multi-band acceleration techniques and the expansion to larger and more diverse patient groups.

KEYWORDS

ADC, diffusion, quantitative, relaxometry, T_1 , Placenta, pregnancy

This is an open access article under the terms of the Creative Commons Attribution License, which permits use, distribution and reproduction in any medium, provided the original work is properly cited.

© 2021 The Authors. *Magnetic Resonance in Medicine* published by Wiley Periodicals LLC on behalf of International Society for Magnetic Resonance in Medicine

1 | INTRODUCTION

The human placenta is of key importance for any successful pregnancy. Major pregnancy complications such as fetal growth restriction (FGR) or pre-eclampsia (PE) have been linked to placental insufficiency with biological and histopathological evidence.^{1,2} The placenta is an exchange organ, composed of 10–40 functional units. The macro- and microstructure of the placenta, especially the fetal vasculature organized in so called villous trees, undergoes dramatic physiological changes to adapt to the needs of the maturing fetus. The fetoplacental compartment is well isolated to protect the growing fetus from external influences and thus difficult to access, noninvasive imaging techniques are therefore ideally suited to gain insights. While ultrasound and Doppler ultrasound are key screening tools, the opportunities to gain functional and structural understanding have led to an increase in in utero MRI imaging—especially quantitative MRI techniques such as relaxometry and diffusion-weighted MRI (dMRI).^{3,4}

T_2^* mapping has been the most frequently used⁵ relaxometry approach in the human placenta in vivo to date, due to both the link to the concentration of deoxygenated hemoglobin (BOLD effect) as well as a large number of readily available acquisition techniques. T_1 mapping, on the other hand, can be used to characterize tissue via its dependency on the molecular environment. Edema, protein deposition, and fibrosis⁶ have all been shown to increase T_1 , whereas deposits of fat and iron shorten T_1 .⁶ T_1 relaxometry has been previously used to study the placenta.^{7–10} However, T_1 values over gestation have not been consistent in previous studies with the results varying from a decrease over gestation^{7,11} to no significant change being identified.⁸ Furthermore, a negative correlation between the difference between R_1 , with $R_1 = 1/T_1$, during norm- and hyperoxygenation (referred to as ΔR_1) was illustrated. A further reduction in ΔR_1 for FGR cases was equally found.^{8,9} T_1 values show, in general, strong quantitative relationships to blood oxygen saturation^{12,13} and were shown to improve the detection of FGR over T_2^* alone⁸ thus highlighting a complementary role. These studies focused on FGR and uncomplicated pregnancies till date and have not included participants with PE. However, histological evidence shows increased fibrin deposition in PE placentas.¹ Fibrin deposition has been successfully interrogated using T_1 mapping in myocardial fibrosis and therefore constitutes a potential avenue for assessing the placenta.

Look-Locker echo planar imaging (EPI),⁷ inversion recovery (IR)^{7–9} using between 4 and 8 inversion times (TI), 3D variable flip angle RF-spoiled gradient spin echo using 3 flip angles¹¹ and most recently MR fingerprinting¹⁰ have all been used to acquire T_1 information in the placenta. However, one significant limitation and challenge for the wider use is the intrinsic inefficiency. Data, for example, from traditional IR

sequences are acquired at a range of TIs by changing the time between the inversion pulse and the excitation, introducing periods of scanner inactivity while waiting for spin relaxation to progress at the specified imaging location. This approach leads to a major problem for fetal and placental imaging as the extended acquisition time allows more time for fetal/placental motion. This motion produces spatial displacement between each TI measurement resulting in errors that reduce the accuracy of the obtained quantitative data.

Diffusion weighted MRI (dMRI) has been used successfully on the human placenta to study the placental microstructure, enabling quantitative tissue measurements such as the density of the villous trees.^{3,14–16} A clinical application of this information has been demonstrated where dMRI imaging was used to quantify the differences between healthy placentas and placentas affected by PE or FGR. Traditionally, placental dMRI datasets are acquired using single-shot diffusion-weighted spin-echo EPI techniques. The single-shot approach to imaging acquires a single slice faster than the tissue displacement, freezing the motion within individual slices. Widely used indices such as the apparent diffusion coefficient (ADC), fractional anisotropy (FA),¹⁷ and complex models¹⁶ have been employed to produce quantitative values for assessment of the placental microstructure.

The need for multiple contrasts to investigate the complex pathophysiology of placental disease and the interconnected functional and structural changes has been widely acknowledged. However, the studies combining multiple contrasts to date have used separate acquisitions for each contrast⁴—thus decreasing spatial data consistency and limiting the ability to study changes on a voxel level. Furthermore, separate acquisitions are not well suited for the highly dynamic nature of in utero imaging, such as contractions, fetal/maternal motion, and vascular/amniotic flow patterns. Our group has previously presented joint T_2^* -diffusion placental imaging³ together with new abilities to represent this data to reveal disease-specific phenotypes and combined perfusion- T_2^* imaging.¹⁸ Previous attempts to accelerate T_1 mapping techniques include slice shuffling approaches, which enable the acquisition of data at multiple TIs in a fast and efficient way.^{17,19,20} For the adult brain, we have expanded upon this with the ZEBRA technique. ZEBRA has been previously proposed as a framework allowing data acquisition in a large parameter space spanned by inversion time, echo time, and diffusion preparation. This was achieved by combining a diffusion-prepared spin-echo sequence with multiple gradient echo read-outs, a global adiabatic inversion pulse and both diffusion and slice shuffling to increase efficiency. The focus for the ZEBRA development so far has been on acquiring comprehensive datasets densely sampling the parameter space in a regime where minimal motion prevails, where acquisition times >10 minutes are acceptable and where the exploration of the data was the focus. However, the aim of this present study is different: The focus

is both to explore fast combined placental dMRI- T_1 in the human placenta and to show first results of this technique in a cohort of women with PE. For this aim, the ZEBRA technique has been changed specifically to fit these requirements and to demonstrate its potential to assess the placenta in healthy pregnancies and those affected by PE.

2 | METHODS

A diffusion-weighted single-shot EPI sequence (ssEPI) was modified previously¹⁷ to include efficient T_1 sampling. Conventionally, ssEPI dMRI techniques acquire all slices consecutively to achieve one volume with the same diffusion weighting in one repetition time (TR). To add T_1 weighting, a global adiabatic inversion pulse was added before the first excitation in each TR assuring that each slice sampled in subsequent excitations during the TR are acquired with a different TI.¹⁹ The sequence also shuffles the applied diffusion weighting on a slice rather than volume level.^{17,21} This results in a sequence where each slice is sampled with each b-values at a subset of TIs. This process is shown in Figure 1 for the 2 b-values and 20 TIs employed for this study both schematically Figure 1A and illustrating the interleaving required for the efficient acquisition in a sagittal reformatted view in Figure 1B.

2.1 | Data acquisition

Datasets were acquired from 43 fetal scans on a clinical 3T Philips Achieva scanner with a 32-channel cardiac coil as part of a larger study (www.placentaimagingproject.org). Informed consent was obtained from all participants according to local procedures (REC 19-SS-0032, 14/LO/1169 and 19/LO/0852). After an initial left lateral preparation to reduce

the potential effects of compression of the vena cava, women were slowly moved into supine position. Dedicated padding, continuous monitoring of the maternal heart rate, blood pressure and oxygen saturation, regular verbal communication and limitation of the scan time to 60 minutes ensured maternal comfort. The dMRI- T_1 datasets described here were acquired in the second half. This approach was tolerated by all participants and life monitoring was uneventful.

The selection of the considered scans is depicted in Figure 2. A total of 43 eligible scans consists of participants considered either “Normal” controls or diagnosed with PE. However, this number was reduced as some of the control cases developed FGR, gestational diabetes mellitus, or gestational hypertension between the time of scan and the delivery and/or delivered before 36 weeks with a neonatal birthweight lower than the third or larger than the 97th centile. Five additional scans were excluded due to visible artifacts from fat aliasing or severe motion. One example for such a scan is shown in Supporting Information Figure S1. Finally, 3 of the control and 2 of the PE scans were removed as these belonged to the same pregnancy scanned times. Therefore, 27 participants with one scan each were finally included into the study, split into 23 healthy participants and 4 participants diagnosed with PE. The location of the placenta, as diagnosed by standardized clinical ultrasound between 19+6 and 21+6 weeks gestation was classified into mostly anterior and mostly posterior cases to form labels with similar geometry with regard to the MRI hardware. In 4 scans, the ZEBRA T_1 -Diffusion sequence was repeated twice during the same examination to assess robustness.

A main magnetic field (B_0) map was acquired prior to EPI scanning to enable image-based shimming.²² An in-house tool connected to the scanner software allows segmentation of the placenta using predefined ellipsoids, calculates second-order shim coefficients and transfers these back to the MRI system. The described ZEBRA sequence was performed in

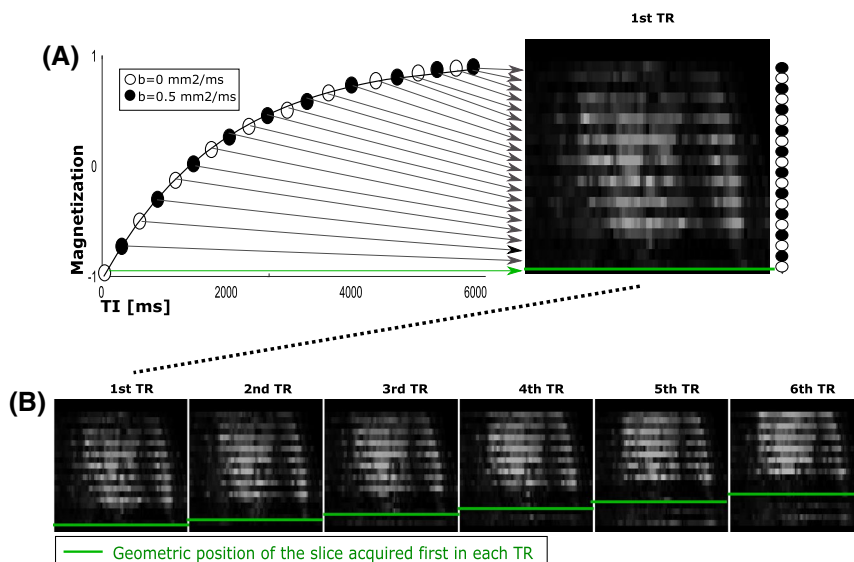


FIGURE 1 Schematic depiction of the proposed T_1 -diffusion sequence, illustrated with a reformatted sagittal view through the fetal brain. A, Inversion curve together with the interleaving of both b-values is depicted. B, Reformatted sagittal views from the first 6 TRs are shown, thereby, the first image corresponds to the previously one shown in (A). The green line shows the spatial position of the first slice acquired in each TR

the scanner axial plane with the center in the field of view aligned roughly with the centre of the placenta. The parameters were optimized to ensure acceptable (<100 dB (A)) acoustic noise, measured as described previously.²³ This effectively increased the required echo spacing in the EPI echo train to reduce the gradient slew rate. Final parameters include resolution $(3\text{ mm})^3$, matrix size 164×164 , SENSE = 2, TR = 6000 ms, TE = 71.7, TIs between 20 and 5674 ms, b-value 0 ms/mm^2 and 0.5 ms/mm^2 .

2.2 | Processing and evaluation

Manual masks were drawn on the volume with the highest contrast (longest TI and $b = 0$) for all slices, giving a conservative segmentation of the placental parenchyma. For relaxometry mono-exponential voxelwise fitting was performed using Equation (1) on a subset of the image data without diffusion weighting ($b = 0$). The full dataset was then modeled using Equation (2) for joint T_1 /ADC quantification. To improve the robustness of the model, 10-fold random initialization was employed, alternating the T_1 start value from $[0-3000]$ ms and ADC from $[0-3]$ ms/mm^2 . The median value resulting from all initialization parameters was obtained and taken as the measured value. Linear regression was performed to detect trends with increasing gestational age and differences between the healthy and PE groups. Two-way ANOVA analysis was performed to assess the significance of changes between both cohorts and GA. As stated

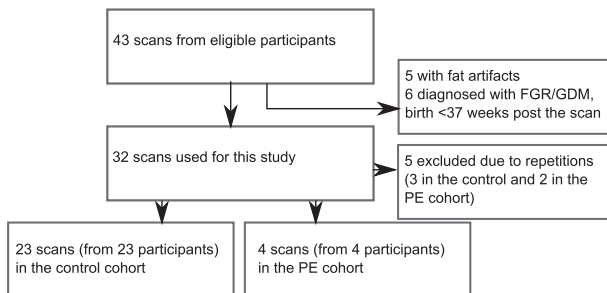
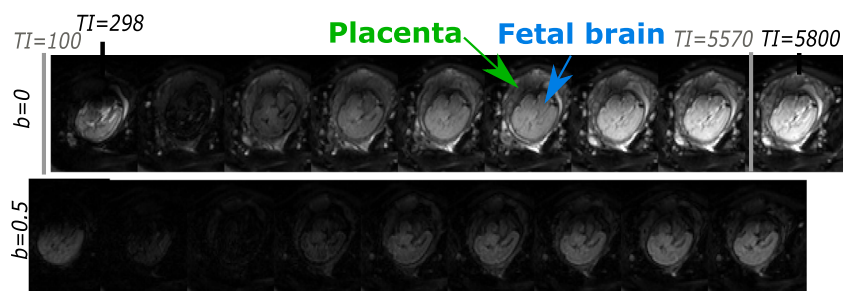


FIGURE 2 Overview of the data collection. The flowchart illustrated the information on how 43 scans from eligible participants reduced to 27 considered scans split into 2 groups of 23 participants in the control group and 4 participants in the PE group

FIGURE 3 Exemplary acquired dMRI- T_1 dataset. The central slice containing the fetal brain and the placenta is illustrated for all TIs from TI = 100 till TI = 5800 and both b-values ($b = 0\text{ ms/mm}^2$ and $b = 0.5\text{ ms/mm}^2$)



above, one scan was used wherever multiple were available for a participant. This has been maintained for the statistical evaluation as well.

$$S_{t1}(TI) = S_0 \left(1 - 2 \left(\exp \frac{-TI}{t1} \right) + \exp \frac{-TR}{t1} \right) \quad (1)$$

$$S_b(TI, b) = S_0 \left(1 - 2 \left(\exp \frac{-TI}{t1} \right) + \exp \frac{-TR}{t1} \right) \exp(-bADC) \quad (2)$$

3 | RESULTS

Combined dMRI- T_1 datasets were successfully acquired in all participants. Data from 1 participant is illustrated in Figure 3 depicting 1 slice for all TIs and both b-values. Obtained placental T_1 and ADC using the joint analysis (Equation 2) maps are shown in Figure 4 the mid-slices for 6 participants are overlaid on the volume with the highest signal. These illustrate a rim of higher ADC on the chorionic plate—indicated with a blue line—as well as cross-placental longitudinal regions of higher ADC. Circular structures with lower ADC values of around $1.5\text{ mm}^2/\text{s}$ in the center can be observed. The T_1 maps show a rim of lower T_1 on the chorionic plate with stripes of higher T_1 —similar to these observed for the ADC but not co-localized. Over gestation an increase in heterogeneity can be observed with increasing areas depicting low signal intensity. Six scans with PE are included (GA 22–29 weeks) with one participant having had 3 scans. While the first acquired at GA 22+6 weeks shows a homogeneous appearance, which corresponds to the quantitative result of mean T_1 and ADC within the normal range (see Figure 5), the other 2 cases exhibit clear differences: Larger regions with reduced ADC and T_1 and a more heterogeneous appearance can be observed overall. Foci with very low ADC ($<1\text{ mm}^2/\text{s}$) can be observed in both cases in the ADC maps, the T_1 maps depict increased heterogeneity and small areas with increased T_1 values (>1200 ms) surrounded by large areas with reduced T_1 values.

Figure 5 depicts the obtained mean quantitative values over GA for all participants, with the participants with PE

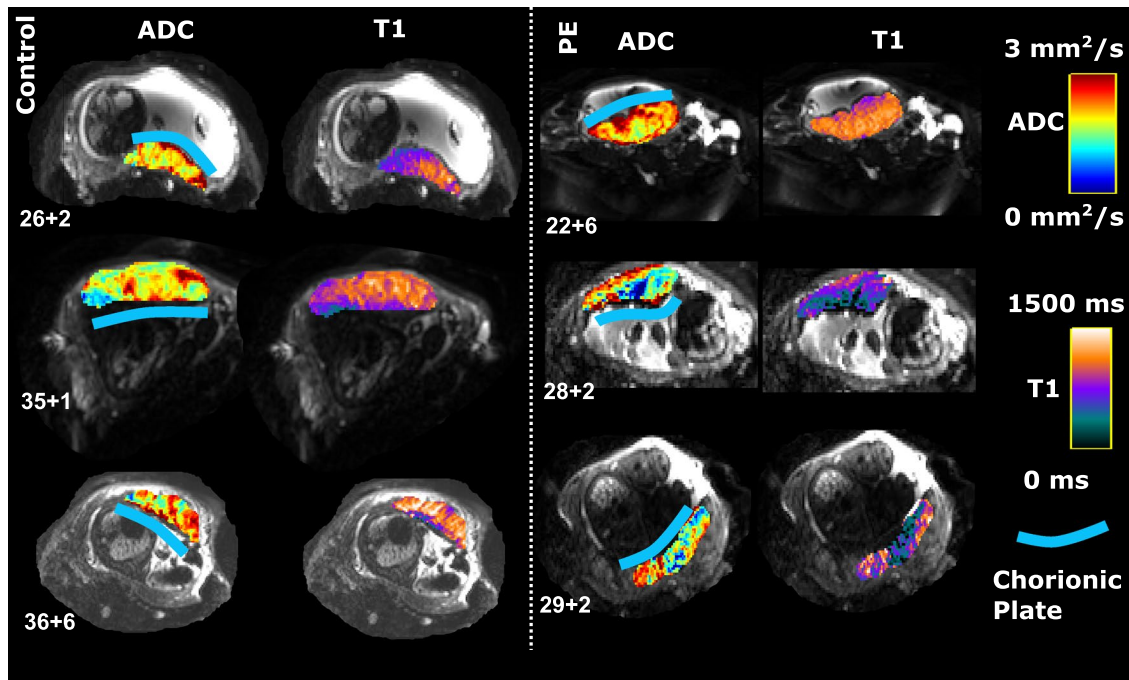


FIGURE 4 Qualitative illustration of the obtained ADC and T_1 maps overlaid on the dynamic with the highest signal ($b = 0$, longest T_1) for 6 of the included cases. The 3 participants on the left are from control participants and the 3 on the right from participants diagnosed with pre-eclampsia. Both are ordered by gestational age and the blue line indicates the location of the chorionic plate

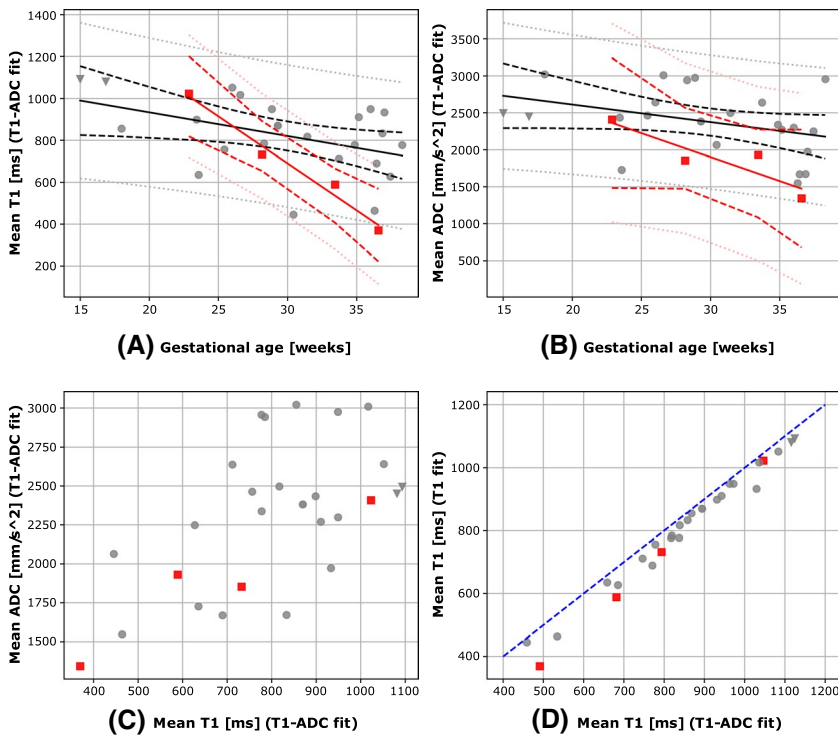


FIGURE 5 Quantitative results from the T_1 -ADC scan. A,B, Mean T_1 and ADC from T_1 -ADC fit over GA, illustrated with the mean confidence interval (dotted) and the lowest and highest confidence interval (striped line). C, Mean T_1 against mean ADC (both from joint T_1 -ADC fit) and D, mean T_1 from T_1 -ADC fit against mean T_1 from T_1 fit. The red squares correspond to the PE participants, gray dots mark the control participants. The dotted blue line in (D) indicates the identity line. Each dot/square in these diagrams corresponds to one scan, as some participants were scanned multiple times as described in the methods. The squares filled with the lighter red are the 3 data points from the same PE participant

colored in red and the healthy control participants in gray. In participants with multiple scans, only the first scan was retained. The mean results from the healthy cohort for the combined ADC- T_1 fit (Equation 2), displayed in Figure 5A,B show a downward trend over gestation for both T_1 (slope -11.3 , $P < .05$) and ADC (slope -0.024 , $P < .1$). The mean

T_1 in the control cohort thereby equaled 1090 ms at 15 weeks GA, 910 ms at 25 weeks GA and 720 ms at 38 weeks GA. The regression analysis for the cohort with placental insufficiency resulted similarly in a downward trend for both T_1 and ADC (TI: slope -44.87 , $P < .05$, ADC: -0.06 , $P = .1$). The correlation between T_1 and ADC from the combined fit is

given in Figure 5C and depicts a linear relationship between both values. The correlation between the T_1 from both fits Equations (1) and (2) in Figure 2D shows that the estimated T_1 values tend to be higher using the joint fit. The data from the participants with repeat acquisitions resulted in a mean deviation of 37.10 ± 14.08 ms in T_1 values. The results of the two-way ANOVA test showed a nonsignificant reduction of ADC and T_1 for the PE cohort.

4 | DISCUSSION AND CONCLUSION

This study explored the use of a technique able to efficiently provide quantitative T_1 and ADC values for the human placenta in vivo in an acquisition time of <2 minutes and demonstrated its ability to discriminate between uncomplicated pregnancies and PE pregnancies. Bespoke to this double aim, a framework able to acquire joint multidimensional data in the diffusion-relaxometry space called ZEBRA, has been successfully adapted. The decreasing trend in ADC value over GA is consistent with previous findings characterizing healthy pregnancies.^{14,18} Prior literature on placental T_1 mapping is sparse⁷⁻⁹ and has not been able to establish clear trends over GA with experiments performed both under norm-oxygenation as in the present study or under hyperoxygenation, where the mother inhales 100% oxygen during the acquisition. A weak negative correlation between GA and T_1 was seen for healthy volunteers,⁸ which is in-line with the results of this study. This could potentially be a consequence of changes in the fraction between maternal and fetal blood and the changing properties of the fetal blood. An increase in fetal hematocrit, as was reported from 0.3 at 17 weeks to 0.45 at 40 weeks was shown to result in a decrease in T_1 similar to the observed.^{13,24} In addition, hematocrit values will change with pathology, eg with chronic hypoxia.²⁵ Similarly, ADC was shown to drop over GA in previous studies—in-line with our results. This might be a consequence of the increase in number of terminal villi and hence in a decrease in average vessel diameter, resulting in additional restriction. Additionally, the fraction of the maternal blood pool decreases, reducing the voxels with significant diffusion to be observed. Following this argument and speculating further, a reduced fraction of maternal blood in the PE cases, might contribute to further pathological decreases in ADC for these cases.²⁶

The need for combined acquisitions and the value offered by a more comprehensive understanding of placental microstructure and function has been recently recognized and explored with joint diffusion- T_2 models⁴ and Diffusion- T_2^* models.³ The present study is to the best of our knowledge one of the first to acquire dMRI and T_1 simultaneously in a combined acquisition. While the proposed ZEBRA technique

has been applied to the adult brain to also achieve T_2^* information by using multiple gradient echos and includes multiple b-vectors enabling more complex modeling and analysis attempts, the focus of this present study was to allow fast, combined quantification of the 2 main parameters, ADC and T_1 . Including multiple echo times would extend the shot length and thus diminish the ability of the technique to sample the TIs densely.

Differences between the T_1 obtained with the 2 considered models illustrate a potential avenue to explore: The estimated T_1 is in general lower if estimated using the joint fit. The shortened T_1 with the joint model is spatially localized in the lobule centers (Supporting Information Figure S2). The presence of a compartment with both high T_1 and ADC would potentially lead to such an effect due to the reduced signal when using higher b-values. Datasets from pregnancies complicated by PE were included largely for illustrative purposes but revealed initial trends of reduced ADC—in-line with literature¹⁶—and reduced T_1 when compared to controls and thus this combined acquisition demonstrates potential to study the microstructural and tissue composition changes involved in these diseases.

This study is a first exploration and presents limitations. First, the chosen orientation of axial to the mother results in a limited placental coverage. With the majority of placentas either dominantly anterior or posterior and thus, this chosen scan orientation is orthogonal to the longest dimension. The large number of slices required to cover the entire placental parenchyma in this orientation while maintaining the present resolution would increase time per volume and thus potentially increase motion artifacts. Future work will thus include multiband techniques.

The foci of this study were both to deliver a clinically feasible fast technique enabling the acquisition of 2 of the previously identified key quantitative values in a short time and to present initial results in participants with PE to evaluate its further use. As a consequence, while the employed sequence was presented before, the design choices are very different with a clear focus on delivering robust and fast measurement of 2 parameters. One resulting limitation is, that only 2 b-values were included. A further extension including more b-values might further increase the robustness and accuracy of the method. Further improved motion correction for example for the maternal respiratory motion is possible due to the interleaving.

The number of participants in the PE group is limited, and, due to the location and parameters of the scanner used, includes mostly late-onset PE cases. This explains the relatively high GA at birth and only slightly reduced mean weight at birth. Due to this and the described focus, we did therefore not include any further clinical outcome evaluation. Applying this technique on a larger and more diverse cohort together with comprehensive clinical outcome and

histopathological results is, however, a next important step. The performed statistical evaluation also needs to be seen with this background in mind and merely constitutes a first evaluation.

ACKNOWLEDGEMENTS

The authors acknowledge the perinatal imaging department and would like to thank the research midwives and radiographers for their contributions. *Acquisition, method, manuscript, and funding:* JH. *Acquisition of the data and manuscript editing:* LJ and PS. *Recruitment of participants and clinical advice:* AH and LS. *Preparation of the manuscript and funding:* JVH, MR, and LC.

ORCID

Jana Hutter  <http://orcid.org/0000-0003-3476-3500>

TWITTER

Jana Hutter  @janahutter

REFERENCES

- Brosens I, Pijnenborg R, Vercruysse L, Romero R. The, "Great Obstetrical Syndromes" are associated with disorders of deep placentation. *Am J Obstetrics Gynecol.* 2011;204:193-201.
- Ho AEP, Hutter J, Jackson LH, et al. T_2 s Placental magnetic resonance imaging in preterm preeclampsia: an observational cohort study. *Hypertension.* 2020;1523-1531.
- Slator PJ, Hutter J, Palombo M, et al. Combined diffusion-relaxometry MRI to identify dysfunction in the human placenta. *Magn Reson Med.* 2019;82:95-106.
- Melbourne A, Aughwane R, Sokolska M, et al. Separating fetal and maternal placenta circulations using multiparametric MRI. *Magn Reson Med.* 2019;81:350-361.
- Sørensen A, Hutter J, Seed M, Grant PE, Gowland P. T_2^* -weighted placental MRI: basic research tool or emerging clinical test for placental dysfunction? *Ultrasound Obstetrics Gynecol.* 2020;55:293-302.
- Bull S, White SK, Piechnik SK, et al. Human non-contrast T_1 values and correlation with histology in diffuse fibrosis. *Heart.* 2013;99:932-937.
- Gowland PA, Francis ST, Duncan KR, et al. In vivo perfusion measurements in the human placenta using echo planar imaging at 0.5 T. *Magn Reson Med.* 1998;40:467-473.
- Ingram E, Morris D, Naish J, Myers J, Johnstone E. MR imaging measurements of altered placental oxygenation in pregnancies complicated by fetal growth restriction. *Radiology.* 2017;285:953-960.
- Huen I, Wright C, Parker G, Sibley C, Johnstone E, Naish J. R_1 and R_2^* changes in the human placenta in response to maternal oxygen challenge. *Magn Reson Med.* 2013;70:1427-1433.
- Stout JN, Rouhani S, Liao C, et al. Placental MRI: using a novel ex vivo placental perfusion chamber to validate in vivo magnetic resonance fingerprinting (MRF) relaxometry. In: Proceedings of the 28th annual meeting of the ISMRM, Montreal (ISMRM 2020). 2020:580.
- Wright C, Morris DM, Baker PN, et al. Magnetic resonance imaging relaxation time measurements of the placenta at 1.5T. *Placenta.* 2011;32:1010-1015.
- Rodríguez-Soto AE, Langham MC, Abdulmalik O, Englund EK, Schwartz N, Wehrli FW. MRI quantification of human fetal O_2 delivery rate in the second and third trimesters of pregnancy. *Magn Reson Med.* 2018;80:1148-1157.
- Portnoy S, Seed M, Sled JG, Macgowan CK. Non-invasive evaluation of blood oxygen saturation and hematocrit from T_1 and T_2 relaxation times: in-vitro validation in fetal blood. *Magn Reson Med.* 2017;78:2352-2359.
- Bonel HM, Stolz B, Diedrichsen L, et al. Diffusion-weighted MR imaging of the placenta in fetuses with placental insufficiency. *Radiology.* 2010;257:810-819.
- Siauve N, Hayot PH, Deloison B, et al. Assessment of human placental perfusion by intravoxel incoherent motion MR imaging. *J Maternal-Fetal Neonatal Med.* 2017;1-8.
- Slator PJ, Hutter J, McCabe L, et al. Placenta microstructure and microcirculation imaging with diffusion MRI. *Magn Reson Med.* 2018;80:756-766.
- Hutter J, Slator PJ, Christiaens D, et al. Integrated and efficient diffusion-relaxometry using ZEBRA. *Sci Rep.* 2018;8:15138.
- Hutter J, Slator PJ, Jackson L, et al. Multi-modal functional MRI to explore placental function over gestation. *Magn Reson Med.* 2019;81:1191-1204.
- Ordidge RJ, Gibbs P, Chapman B, Stehling MK, Mansfield P. High-speed multislice T_1 mapping using inversion-recovery echo-planar imaging. *Magn Reson Med.* 1990;16:238-245.
- Wu H, Tian Q, Poetter C, et al. Whole brain inversion recovery diffusion weighted imaging using slice-shuffled acquisition. In: *ISMRM 2017.* 2017:387.
- Hutter J, Christiaens DJ, Schneider T, et al. Slice-level diffusion encoding for motion and distortion correction. *Med Image Anal.* 2018;48.
- Gaspar A, Ferrazzi G, Nunes R, et al. Improving functional imaging of the fetal brain using constrained image-based shimming to suppress maternal fat. In: Proceedings of the 24th annual meeting of the ISMRM, Singapore, May 07- 13 (ISMRM 2016). 2016:4303.
- Hutter J, Price AN, Cordero-Grande L, et al. Quiet echo planar imaging for functional and diffusion MRI. *Magn Reson Med.* 2018;79:1447-1459.
- Xu J, Duan AQ, Marini D, et al. *The utility of MRI for measuring hematocrit in fetal anemia.* 2020;222:81.e1-81.e13.
- Zhu MY, Milligan N, Keating S. The hemodynamics of late-onset intrauterine growth restriction by MRI. *Am J Obstetrics Gynecol.* 2016;214:367.e1-367.e17.
- Jackson MR, Mayhew TM, Boyd PA. Quantitative description of the elaboration and maturation of villi from 10 weeks of gestation to term. *Placenta.* 1992;13:357-370.

SUPPORTING INFORMATION

Additional Supporting Information may be found online in the Supporting Information section.

TABLE S1 Brief description of the considered control and PE cases. The mean values are given for gestational age at scan, maternal age and BMI as well as gestational age and weight at birth

TABLE S2 All considered PE data points. Thereby, the line written in italic highlights the participant with 3 scans.

The GA written in bold corresponds to the scan of this participant displayed in the figures

FIGURE S1 Illustration of one case which was excluded due to unresolved fat artifacts

FIGURE S2 Illustration of the different T_1 maps achieved with the T_1 fit using only the data acquired at $b = 0$ and the joint T_1 ADC fit on the entire data together with the difference map on the right

How to cite this article: Hutter J, Ho A, Jackson LH, et al. An efficient and combined placental T_1 -ADC acquisition in pregnancies with and without pre-eclampsia. *Magn Reson Med*. 2021;86:2684–2691. <https://doi.org/10.1002/mrm.28809>